Mesophase as the Precursor for Strain-Induced Crystallization in Amorphous Poly(ethylene terephthalate) Film

Shaofeng Ran, Zhigang Wang, Christian Burger, Benjamin Chu,* and Benjamin S. Hsiao*

Department of Chemistry, State University of New York at Stony Brook, Stony Brook, New York 11794-3400

Received August 2, 2002; Revised Manuscript Received October 21, 2002

ABSTRACT: An in situ study of strain-induced crystallization in an amorphous poly(ethylene terephthalate) (PET) film was carried out by using wide-angle X-ray diffraction with synchrotron X-rays. Results indicated that the mesophase was developed during stretching, immediately upon necking below T_g. A sharp meridional peak was observed during the mesophase formation. The *d*-spacing (10.32 Å) of this peak was smaller than the monomer length, indicating that the chains in the mesophase could be tilted with respect to the stretching direction. Prior to crystallization, the intensity of this peak was found to increase upon stretching. The triclinic PET crystalline structure began to form as the temperature was increased above T_g. Then, the corresponding intensity of the $d = 10.32$ Å peak was found to decrease. This observation suggests that the triclinic PET crystals form an inclined layered structure, which shifts this peak out of the meridian. A two-dimensional analytical method was used to deconvolute the diffraction pattern into isotropic and anisotropic contributions. The isotropic and anisotropic fractions remained almost constant after stretching was stopped and during crystallization, suggesting that the strain-induced crystallization occurs mainly in the mesophase, supporting the hypothesis that the intermediate mesophase acts as a precursor for crystallization in oriented PET.

Introduction

Poly(ethylene terephthalate) (PET) is one of the most commercially important polyesters. As the polymer has to be processed by flow or deformation in the molten or solid state, the strain-induced crystallization behavior in this polymer is of both academic and industrial interest. In this study, we are interested in the strain-induced crystallization from the glassy solid, which has also attracted the attention of many research groups.[1−15]

Upon crystallization, PET forms a triclinic unit cell with $a = 4.56$ Å, $b = 5.94$ Å, $c = 10.75$ Å, $\alpha = 98.5°$, $\beta = 118°$, and $\gamma = 112°$.[3] Upon stretching, this crystal structure can be deformed. Zimmermann et al. reported that stretching of semicrystalline PET caused changes in *d*-spacings of the (100) and (010) planes.[4] Porter et al. observed that the lattice parameters of stress-induced crystallites in PET were different from those in the closest packing.[5] However, PET can also form an amorphous glass. Bonart was the first scientist who reported the formation of a "paracrystalline" structure in PET induced by drawing.[7] He observed that the structure of PET changed during stretching of a totally amorphous sample, first forming a nematic phase and then a smectic phase. Here and below, we follow the terminology of the original authors to call these lattice distortions "paracrystalline" although it has been shown a long time ago that the paracrystalline model of disorder breaks down in more than one dimension.[8,9] Yeh and Geil pointed out that the quenched amorphous PET consisted of granulelike structures in which molecules exhibited a paracrystalline order, based on their electron microscopic observation.[10,11] They argued that strain-induced crystallization could be explained by rotation, alignment, and perfection of the internal order of the paracrystalline granulelike structure. Windle et al. recently reported the formation of a transient smectic phase in the fiber made of random PET and PEN (polyethylene naphthalene-2,6-dicarboxylate) copolymers.[12] Balta Calleja et al. investigated the structural changes during annealing of cold-drawn amorphous PET films by X-ray diffraction and microindentation techniques.[13] Their results revealed the appearance of a smectic order at 60 °C having a spacing of 10.7 Å. Recently, Blundell et al. studied the in situ structural development of PET films during fast-drawing using synchrotron X-ray techniques.[1,14−15] Their results indicated a strong dependence of the crystallization rate on both temperature and molecular orientation. They also observed a highly oriented weak transient diffraction peak on the meridian prior to crystallization and identified it with the mesophase structure. They suggested that this transient structure was a precursor for strain-induced crystallization.

In this study, we are particularly interested in understanding the relationships between the mesophase and the crystallization in PET during deformation. We have devised two different stages in the experiments: (1) the deformation of an amorphous PET sample at a constant velocity below T_g and (2) the crystallization of a deformed sample at a constant strain at different temperatures. The structural changes were followed by the in situ synchrotron wide-angle X-ray diffraction (WAXD) technique. Some new evidence has been gathered, which supported the hypothesis that the mesophase is the precursor for crystallization during deformation in PET. In fact, we did not observe that additional crystallization occurred directly from the amorphous phase.

Experimental Section

A modified Instron 4410 stretching apparatus was adapted to a three-pinhole collimated X-ray facility at the X3A2

* To whom correspondence should be addressed. E-mail: bchu@notes.cc.sunysb.edu; bhsiao@notes.cc.sunysb.edu.

10.1021/ma021252i CCC: $22.00
Published on Web 12/07/2002

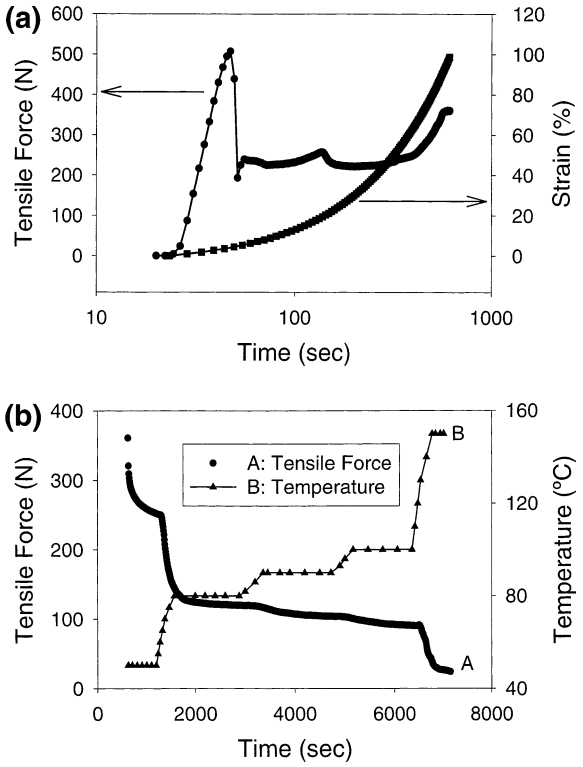

Figure 1. Variations of applied stress and strain vs time for the PET film during (a) deformation at a constant rate and (b) crystallization at a fixed strain.

beamline (λ = 1.54 Å) of the National Synchrotron Light Source (NSLS), Brookhaven National Laboratory (BNL), to perform the in situ WAXD study. The modification of the Instron instrument allowed the sample to be stretched symmetrically, which assured that the focused X-ray beam always illuminated the same position on the sample during deformation.

A completely amorphous PET film obtained from the Mitsubishi Chemical Co. was used in this study. The amorphous structure was verified by a differential scanning calorimetry (DSC) scan under a nitrogen environment. The deformation and crystallization studies were carried out using the following two procedures. (1) The amorphous sample was first stretched to an extension of 100% at a constant crosshead speed of 10 mm/min at 50 °C. (2) The stretched sample was then heated to four different temperatures (80, 90, 100, and 150 °C) at a rate of 5 °C/min under a constant strain. At each temperature stage, the sample was held for about 20 min before heating to a higher temperature. Two-dimensional (2D) WAXD patterns were accumulated over periods of 25 s using a charge-coupled device (CCD) X-ray detector (MARUSA) during both processes 1 and 2. The distance from the CCD detector to the sample was 114.1 mm. The diffraction angle was calibrated by an Al_2O_3 standard from the National Institute of Standards and Technology (NIST). The stress−strain curve was recorded automatically during the deformation and crystallization processes.

Results and Discussion

Figure 1 shows the variations of applied stress and strain versus time in the two different stages of (a) deformation at a constant stretching rate and (b) crystallization under a constant strain at different temperatures, respectively. In Figure 1a (the deformation stage), multiple singularities in the stress curve correspond to the multiple necking events occurring during the stretching process. It is quite interesting to note that stress continued to rise after the necking until 625 s when stretching was stopped and strain reached

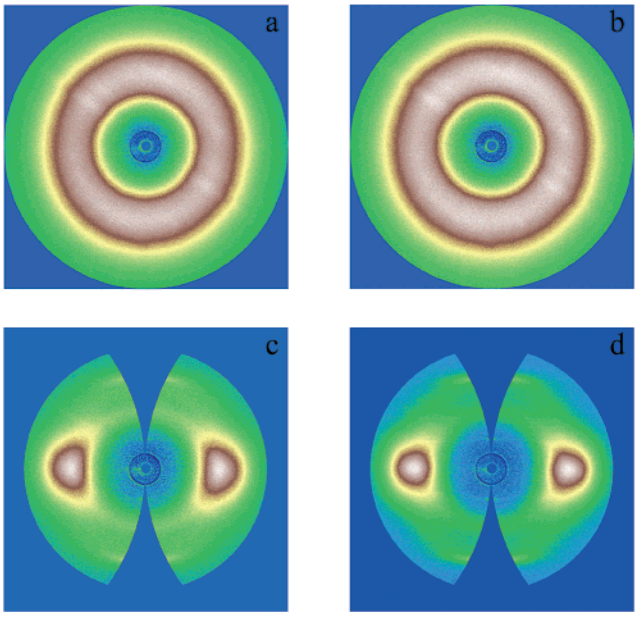

Figure 2. 2D WAXD patterns (geometrically corrected for distortion due to the curvature of the Ewald sphere, except patterns a and b) at different deformation stages at 50 °C: (a) strain = 0%, 0 s; (b) strain = 20%, 125 s; (c) strain = 58%, 375 s; (d) strain = 100%, 625 s.

the 100% level. On the basis of the WAXD data shown later, the material was partially transformed into a mesomorphic phase at this point. Figure 1b shows the changes of applied stress and temperature during crystallization of the stretched PET (mesomorphic) sample that was kept at a constant strain. The stress was decreased quite substantially, corresponding well to the changes in temperature. Four break points of the applied stress were observed, coinciding with the temperature changes at 80, 90, 100, and 150 °C.

On the basis of similar WAXD patterns taken in the face-on and the edge-on directions, we can assume that the film sample has fiber symmetry, with the fiber axis along the stretching direction (meridian) and the equator perpendicular to it. Two-dimensional WAXD patterns in the undistorted reciprocal space at different deformation stages are shown in Figure 2, after corrections for the air scattering and the instrumental background scattering. These diffraction patterns (except Figure 2a,b where the patterns are isotropic) represent the geometrical correction of the flat-plate images due to the detection distortion by the curvature of the Ewald sphere.[16] The isotropic scattering feature in Figure 2a indicated that the initial PET sample was completely amorphous with no preferred orientation. When the strain reached the value of 58%, the isotropic amorphous scattering ring was seen to converge into a pair of broad and intense arcs on the equator (Figure 2c). In Figure 2c, an additional pair of weak but distinct peaks (2θ = 8.56° and 26.10°) was also observed on the meridian immediately after the structural change. The absence of crystalline order in the interchain packing in Figure 2c indicates that a mesophase structure (e.g., nematic or smectic) is formed as was reported in the literature.[12] This mesomorphic structure has a degree of packing order that is between the crystalline phase and the amorphous phase. We observed the mesophase only when the X-ray irradiated volume coincided with the neck region, which might be the reason we did not see any structural changes in Figure 2b (strain = 20%).

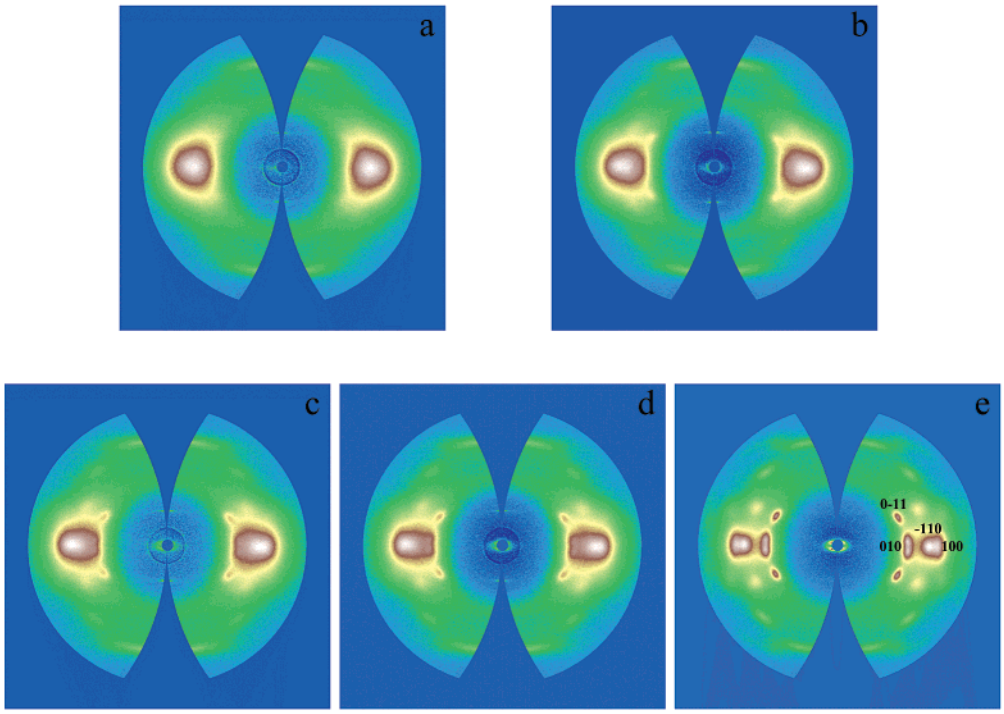

Figure 3. 2D WAXD patterns (geometrically corrected for distortion due to the curvature of the Ewald sphere) during crystallization at different temperatures under a constant strain (=100%): (a) 50 °C, (b) 80 °C, (c) 90 °C, (d) 100 °C, and (e) 150 °C.

As a result, the exact strain required for the formation of the mesophase cannot be determined in the present study. Figure 2d represents the WAXD pattern collected during the maximum strain (100%) used in the study, which shows no sign of crystallization. The total diffraction intensity of the mesophase (i.e., the sum of the intensities from three anisotropic reflection peaks at about 8°, 18°, and 26°) was found to increase with increasing strain.

The crystallization results from the heating of the stretched sample under a constant strain are shown in Figure 3. In Figure 3b, it is seen that when the temperature was increased to 80 °C (just above T_g), the broad equatorial peak began to split into several distinct crystal reflections on the equator and four weak reflections ($0\bar{1}1$) off the equator axis.[17] These peaks indicate that PET started to crystallize into a triclinic unit cell with distinct three-dimensional packing order. With the further increase in temperature, more off-axis reflections were seen and their intensities also became stronger (Figure 3c−e), indicating that the crystallinity was increased and the crystallites became more perfect by high-temperature annealing. In Figure 3, all patterns showed crystal reflections as sharp spots, indicating that the formed crystallites were well oriented in the stretched sample under constant strain. The degree of orientation was about the same in all the patterns. In Figure 3e, it is seen that the 010 reflection was actually not on the equator. It split into two peaks displaced up and down from the equator. This result confirms that the *a*−*c*-plane in real space and, thus, the *c*-axis of the triclinic PET crystal are tilted with respect to the stretching direction, which has been well documented for PET[3] and has also been seen in other triclinic polyesters.[18]

Figure 4 illustrates the linear meridional intensity profiles at different stages of deformation and of crystallization, respectively. These one-dimensional (1D) intensity profiles were calculated from the flat-plate

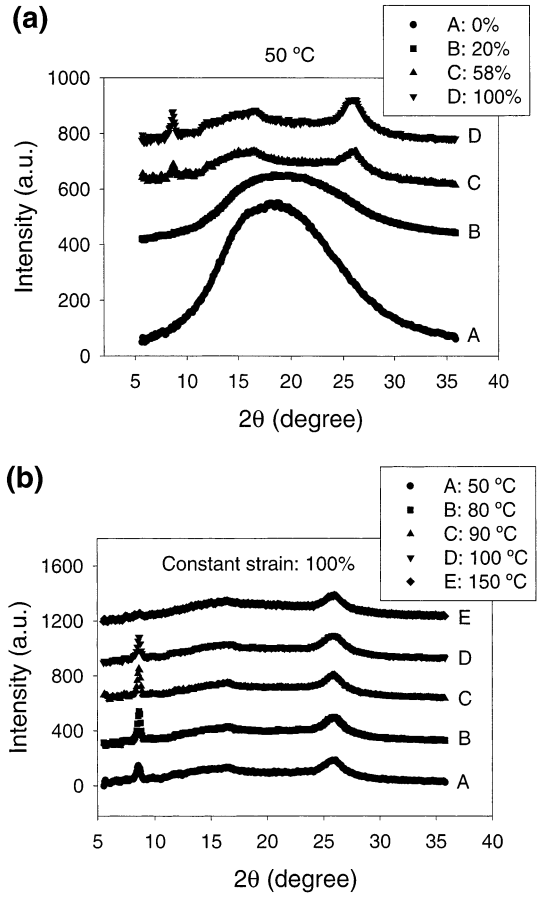

Figure 4. 1D intensity profiles on the meridian calculated from the flat-plate 2D WAXD images (by azimuthal averaging from 85° to 95°) of the PET film. (a) At different deformation stages: strain = 0%, 20%, 58%, and 100%. (b) At different temperatures (under a fixed strain): 50, 80, 90, 100, and 150 °C. (Plots are vertically shifted for visual separation.)

WAXD images by azimuthal averaging from 85° to 95° on the meridian. In Figure 4 (during deformation at a constant rate), only a broad scattering peak (at 2θ of about 18°) was seen before the strain reached 58%. This broad peak is due to the amorphous chain interactions. The amorphous peak became slightly broader at a strain of 20% (the full width at half-maximum changed from 13.2° to 13.8°), and the peak position shifted to a higher scattering angle (lower *d*-spacing). Perhaps, this indicates that the stretching process densifies the packing of amorphous chains. As the necking region reached the irradiated detection spot, three distinct peaks were seen. The *d*-spacing of the peak at the highest measured angle was 3.41 Å. The *d*-spacing of the peak at the lowest measured angle was 10.32 Å. With increasing strain or temperature, the position of the peak at $d = 3.41$ Å remained constant even when PET was being crystallized (Figure 4b). This result implies that the chains in the mesophase may already have a similar packing symmetry as in the crystalline phase.

An interesting observation is made during the changes of the peak with $d = 10.32$ Å (we term it 001′ here). The intensity of this peak increased rapidly during the deformation stage (Figure 4a). During the crystallization stage, the intensity of this peak reached the maximum value at about 80 °C (when crystallization occurred) and then it started to decrease (Figure 4b). The peak position remained constant during both processes (deformation and crystallization). A qualitatively similar behavior has been reported before.[1,12−13] However, the reported *d*-spacings of this peak were found to be different, namely, 11.5 Å for the PET/PEN copolymer[12] and 10.7 Å[13] and 10.2 Å[1] for PET homopolymers. Windle et al. proposed that this peak could be attributed to a smectic A structure (having an untilted mesogen arrangement).[12] Since the monomer length of PET (in the triclinic unit cell) is 10.75 Å, the chains in the mesophase must be packed approximately parallel to the stretching direction as in the case of the smectic A structure. However, the *d*-spacing of the present peak was 10.32 Å, which was shorter than the monomer length. There are several possibilities for the chain packing in this case. The simplest one is that all the chains are parallel to the stretching direction and form perpendicular layers, and the monomer period is reduced by conformational changes, for example, gauche sequences in the ethylene group, which could cause the decrease in d_{001}. However, this model appears to be unlikely for a stretching process (i.e., stretching decreases the monomer length). The second possibility is that all the chains are parallel to the stretching direction, but they form inclined layer structures. The schematic diagram of this model is shown in Figure 5a. In this case, the meridional peak 001′ should split into two peaks with $d_{001'} = 10.32$ Å due to the inclined layers. However, we did not observe any split of this peak, which contradicts this model. Therefore, the most likely packing scenario for the chains is to form a smectic C structure; that is, the chain axes have a tilt angle with respect to the stretching direction, but the layers are still perpendicular to the stretching direction (Figure 5b). The equatorial peak should split in this model. However, the split peaks may not be distinct enough to be distinguished because they will overlap with each other and/or with the broad mesophase peak on the equator. The formation of the smectic C structure could be explained as follows. As the inclined crystal structure has been reported in the necking region of drawn fibers or films,[19] we could imagine that the shear component during deformation in this region is responsible for the tilting of the chains. Only at high elongations, the chain molecules can be straightened resulting in high axial orientation parallel to the stretch direction,[20] which may have been the case in the fiber study of Windle et al.[12] In the present study, the strain was always kept at a relatively low level such that the tilted structure prevailed.

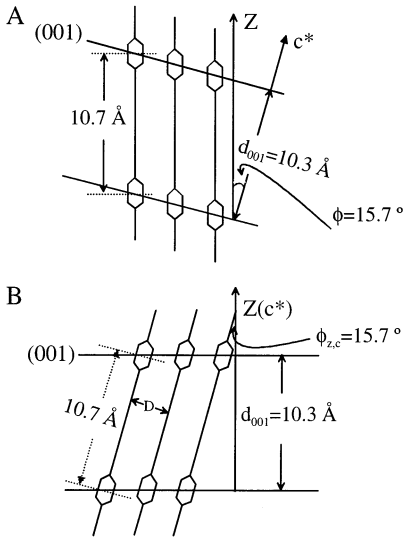

Figure 5. Schematic diagram of two possible packing models for the mesophase in PET. *Z* and *c** represent the stretching direction and the *c**-axis, respectively.

The peak intensity of $d = 10.32$ Å has been found to decrease during crystallization in the oriented sample. It is known from the simulation results that chains form an inclined layer structure with respect to the stretching direction in the PET triclinic crystals, which causes the 001 reflection to be very weak and not on the meridian. With transition from the mesophase to the crystals, more and more chains form triclinic crystals, which shifts the 001 reflection out of the meridian, resulting in a decrease of the 001′ peak. However, there is another possibility that cannot be ruled out. The 001′ peak could (partially) disappear in the region that cannot be detected due to the curvature of the Ewald sphere. By examination of the WAXD patterns in Figure 3, it is clear that the sharper a peak becomes, the more intensity it loses to the undetectable region; eventually, the observable part of a sharp peak will only consist of its weak tails. In Figure 3, there is another sharp peak on the meridian ($2\theta = 26.10°$ or $d = 3.41$ Å), which is related not to the higher order of 001′ but rather to $\bar{1}03$. This reflection lies neither on the crystallographic *c**-axis nor on the axis which is normal to the *a**−*b**-plane (which does not coincide with the *c** for triclinic symmetry and corresponds to the *c*-axis in real space). In the simple fiber symmetry orientation model used here, this reflection is first cylindrically averaged about the axis given by the normal to the *a**−*b**-plane mentioned above and then cylindrically averaged about the main fiber axis. The double averaging results in a broad intensity distribution spanning over the meridian as observed, which makes it less likely to disappear (i.e., it loosely overlaps with the Ewald sphere) when the structural unit (its pole figure) is tilted.

In this study, a two-dimensional analytical method was used to deconvolute the WAXD pattern into two fractions: isotropic and anisotropic parts. The isotropic part includes the scattering from the amorphous phase and has no azimuthal dependence, which can be obtained using a method described as follows. For each absolute value s of the scattering vector ($s = 2\sin(\theta)/\lambda$, 2θ is the scattering angle) in a certain range ($0.056\ \text{Å}^{-1} < s < 0.35\ \text{Å}^{-1}$), the azimuthal scan has been performed on the Fraser-corrected WAXD pattern. Each azimuthal scan curve can be fitted into a Legendre expansion.[21]

$$I(s,\phi) = \sum a_{2n} P_{2n}(\cos\phi) \qquad (1)$$

where P_n is the Legendre polynomial of the first kind of order n. The fit functions are extrapolated into the "missing region", thereby reducing the cutoff error of the integrations. With the obtained coefficients a_{2n}, the minimum a_m can be calculated in each azimuthal scan for different s. All of the minimum intensities at different values of s thus represent the envelope of the isotropic contribution. The anisotropic mass fraction, which is then obtained as the difference between the total intensity and the isotropic intensity, contains the oriented fractions of both the oriented mesophase and the crystals. This procedure slightly underestimates the anisotropic fraction since also in these domains a small part of the molecule happens to be oriented in the perpendicular direction.

As the above procedure was used to analyze the diffraction data at high temperatures, another concern should also be addressed. That is whether a temperature increase will cause the anisotropic scattering to lose a part of its intensity to the isotropic fraction. This can be considered in two aspects. The effect of a temperature increase is that a part of the intensity located in the diffraction peaks goes into the thermal diffuse scattering (TDS), which results in scattering tails to the peaks and an additional scattering background. The overall integrated scattering intensity (invariant) stays, however, constant. For the isotropic scattering contribution, this means that it can change its shape but it will remain isotropic and not change the invariant. For an anisotropic arrangement of polymer chains, a large part of the thermal movement will be anisotropic as well, resulting in anisotropic thermal diffuse scattering. However, there is a certain contribution that may be lost to an isotropic background. Furthermore, a difference in the thermal expansion coefficients of the anisotropic and the isotropic phase can also lead to a shift in their volume fractions. We have assumed both effects to be small and neglected them.

Figure 6 shows the variations of isotropic and anisotropic mass fractions during (a) deformation and (b) crystallization processes. In Figure 6a, it is seen that the structure was totally isotropic in the initial sample. As the neck region moved into the detection spot (t = 325 s), the isotropic fraction decreased dramatically and the anisotropic fraction became larger rapidly in the entire pattern till the extension of 58% (375 s). With a further increase in strain, the anisotropic fraction still increased gradually, indicating that more chains were oriented. This is also consistent with the observation of the increase in the 001′ peak intensity at d = 10.32 Å. We should mention that the natural draw ratio at the necking region is actually larger than 100% (about 150%) due to the necking. In this case, even at the end

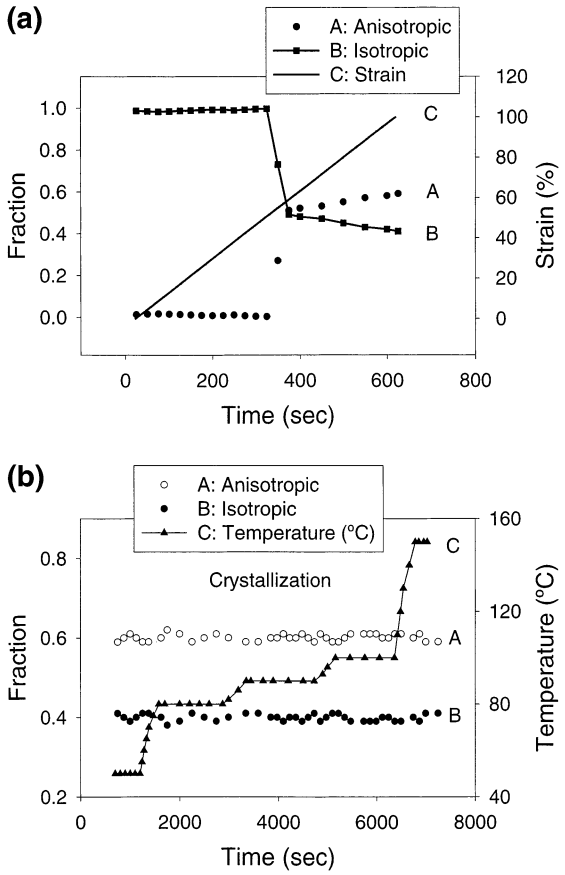

Figure 6. Variations of isotropic and anisotropic mass fractions during (a) the deformation stage and (b) the crystallization stage (at a constant strain).

of stretching, both the drawn region and the undrawn region coexisted. Thus, the additional stretching in the necking region with increasing stretching ratio could be small, which might be the reason that the increase in the anisotropic fraction quickly slowed soon after the dramatic change at the beginning of the necking. It is interesting to note that both anisotropic and isotropic fractions remained about constant in the crystallization stage (Figure 6b). From the above findings, we can make the following conclusion. We believe that the amorphous phase is not converted directly into the crystal phase because the amorphous fraction remains constant during the crystallization stage. This is strong evidence that strain-induced crystallization occurred mainly in the mesophase region that was developed by stretching. It is conceivable that it is much easier for PET molecules in the mesophase to crystallize than for the molecules in the amorphous phase, since the chains in the mesophase have already possessed some arrangement and orientation similar to the molecules in the triclinic crystals. Thus, the formation of the triclinic crystals may occur entirely from the oriented chains in the mesophase. In other words, the mesophase acted as the precursor for strain-induced crystallization and can greatly accelerate the crystallization process. In fact, no additional crystallization occurring directly from the amorphous phase was observed in this oriented sample. This conclusion was first suggested by Shimizu et al.[22] and has recently been confirmed by Windle et al.,[12] our group, and Schultz et al.[23]

Conclusion

Strain-induced crystallization of PET was investigated after an amorphous PET film was stretched to an extension of 100% below T_g using in situ synchrotron WAXD techniques. Results indicated that the mesophase developed immediately upon the neck formation. A sharp meridional peak 001′ (d = 10.32 Å) was observed in the mesophase. The d-spacing of this peak was smaller than the monomer length in the unit cell, which indicated that the chains in the mesophase formed an inclined smectic C structure. The intensity of this peak increased during the mesophase formation and decreased drastically upon the formation of triclinic crystalline structure above T_g. The isotropic fraction in the diffraction pattern was separated from the anisotropic contribution. It was found that both isotropic and anisotropic fractions remained about constant during crystallization at different temperatures. This indicated that strain-induced crystallization occurred mainly in the mesophase region, which supports the hypothesis that the mesophase acts as the precursor for strain-induced crystallization.

Acknowledgment. B.C. and B.H. gratefully acknowledge the financial support of this work by grants from the U.S. Army Research Office (DAAD190010419), the National Science Foundation (DMR9984102), and the U.S. Department of Energy (DEFG 0286 ER45237.016). B.H. also acknowledges the financial support from the NSF Center for Advanced Engineering Fibers and Films at Clemson University. The PET samples were provided by Drs. G. Harrison and D. Edie at Clemson University. The authors also thank Dr. K. H. Gardner and J. Frieda of DuPont Central Research for the assistance of confirming the smectic C structure. The assistance from Dr. Dufei Fang for the X-ray image analysis program is gratefully appreciated.

References and Notes

(1) Mahendrasingam, A.; Martin, C.; Fuller, W.; Blundell, D. J.; Oldman, R. J.; MacKerron, D. H.; Harvie, J. L.; Riekel, C. *Polymer* **2000**, *41*, 1217.
(2) Chang, H.; Lee, K. G.; Schultz, J. M. *J. Macromol. Sci., Phys.* **1994**, *B33* (1), 105.
(3) Daubery, R. D.; Bunn, C. W.; Brown, C. J. *Proc. R. Soc. London, Ser. A* **1954**, *226*, 531.
(4) Sauer, T. H.; Wendorff, J. H.; Zimmermann, H. J. *J. Polym. Sci., Polym. Phys. Ed.* **1987**, *25*, 2471.
(5) Sun, T.; Zhang, A.; Li, F. M.; Porter, R. S. *Polymer* **1988**, *29*, 2115.
(6) Wakelyn, N. T. *J. Appl. Polym. Sci.* **1983**, *28*, 3599.
(7) Bonart, R. *Kolloid-Z.* **1966**, *213*, 1.
(8) Zernike, F.; Prins, J. A. *Z. Phys.* **1927**, *41*, 41.
(9) Bramer, R.; Ruland, W. *Macromol. Chem. Phys.* **1976**, *177*, 3601.
(10) Yeh, G. S. Y.; Geil, P. H. *J. Macromol. Sci., Part B* **1967**, *1*, 235.
(11) Yeh, G. S. Y.; Geil, P. H. *J. Macromol. Sci., Part B* **1967**, *1*, 251.
(12) Welsh, G. E.; Blundell, D. J.; Windle, A. H. *Macromolecules* **1998**, *31*, 7562.
(13) Asano, T.; Balta Calleja, F. J.; Flores, A.; Tanigaki, M.; Mina, M. F.; Sawatari, C.; Itagaki, H.; Takahashi, H.; Hatta, I. *Polymer* **1999**, *40*, 6475.
(14) Blundell, D. J.; Mahendrasingam, A.; Martin, C.; Fuller, W.; MacKerron, D. H.; Harvie, J. L.; Oldman, R. J.; Riekel, C. *Polymer* **2000**, *41*, 7793.
(15) Mahendrasingam, A.; Blundell, D. J.; Martin, C.; Fuller, W.; MacKerron, D. H.; Harvie, J. L.; Oldman, R. J.; Riekel, C. *Polymer* **2000**, *41*, 7803.
(16) Fraser, R. D. B.; Macrae, T. P.; Millar, A.; Rowlands, R. J. *J. Appl. Crystallogr.* **1976**, *9*, 81.
(17) Goschel, U.; Deutscher, K.; Abetz, V. *Polymer* **1996**, *37* (1), 1.
(18) Hall, I. H. *Structure of Crystalline Polymers*; Hall, I. H., Ed.; Elsevier Applied Science: New York, 1984; pp 39−77.
(19) Kakudo, M.; Kasai, N. *X-ray Diffraction by Polymers*; Kodansha Ltd./Elsevier: Tokyo/New York, 1972; pp 405.
(20) Dulmage, W. J.; Geddes, A. L. *J. Polym. Sci.* **1958**, *31*, 499.
(21) Ruland, W. *Colloid Polym. Sci.* **1977**, *255*, 833.
(22) Shimizu, J.; Kikutani, T.; Takaku, A.; Okui, N. *Sen'i Gakkaishi* **1984**, *40* (6), T177.
(23) Wu, J.; Schultz, J. M. Unpublished results.

MA021252I